

# The aspherical explosions of the 03fg-like Type Ia supernovae 2021zny and 2022ilv revealed by polarimetry

T. Nagao,<sup>1,2,3</sup> K. Maeda,<sup>4</sup> S. Mattila,<sup>1,5</sup> H. Kuncarayakti,<sup>1,6</sup> C. P. Gutiérrez,<sup>7,8</sup> and A. Cikota<sup>9</sup>

<sup>1</sup> Department of Physics and Astronomy, University of Turku, FI-20014 Turku, Finland

<sup>2</sup> Aalto University Metsähovi Radio Observatory, Metsähovintie 114, 02540 Kylmälä, Finland

<sup>3</sup> Aalto University Department of Electronics and Nanoengineering, P.O. BOX 15500, FI-00076 AALTO, Finland

<sup>4</sup> Department of Astronomy, Kyoto University, Kitashirakawa-Oiwake-cho, Sakyo-ku, Kyoto 606-8502, Japan

<sup>5</sup> School of Sciences, European University Cyprus, Diogenes Street, Engomi, 1516, Nicosia, Cyprus

<sup>6</sup> Finnish Centre for Astronomy with ESO (FINCA), University of Turku, FI-20014, Finland

<sup>7</sup> Institut d'Estudis Espacials de Catalunya (IEEC), Edifici RDIT, Campus UPC, 08860 Castelldefels (Barcelona), Spain

<sup>8</sup> Institute of Space Sciences (ICE, CSIC), Campus UAB, Carrer de Can Magrans, s/n, E-08193 Barcelona, Spain

<sup>9</sup> Gemini Observatory / NSF's NOIRLab, Casilla 603, La Serena, Chile

Received \*\*\*; accepted \*\*\*

## ABSTRACT

**Context.** A peculiar subtype of Type Ia supernovae (SNe), 03fg-like (super-Chandrasekhar) SNe, show different observational properties from prototypical Type Ia SNe, typically having high luminosity at the light-curve peak, low expansion velocities, and strong carbon features. The origin of this class of Type Ia SNe has been actively debated. Recent nebular-phase infrared observations of the 03fg-like Type Ia SN 2022pul using the James Webb Space Telescope revealed large-scale asymmetries in the ejecta and the presence of the strong [Ne II] line at  $12.81 \mu\text{m}$ , suggesting a violent merger of two white dwarfs as its origin.

**Aims.** Polarimetry is another powerful tool to study overall ejecta asymmetries of spatially-unresolved SNe. Here, we aim to check the universality of the violent merger scenario as the origin of the 03fg-like Type Ia SNe, by studying their explosion geometries using polarimetry.

**Methods.** In this letter, we present imaging-polarimetric observations of the two 03fg-like Type Ia SNe 2021zny and 2022ilv.

**Results.** SNe 2021zny and 2022ilv show high intrinsic polarization ( $\sim 1\% \sim 2\%$ ), which might be composed of multiple components with different polarization angles. This indicates that they have complex aspherical structures in their ejecta, supporting the violent merger scenario for their origin. Our observations provide the first clear evidence from polarimetry for such aspherical structures.

**Key words.** supernovae: individual: SN 2021zny – supernovae: individual: SN 2022ilv – Techniques: polarimetric

## 1. Introduction

Type Ia supernovae (SNe) are explosions of white dwarfs (WDs), powered by runaway thermonuclear burning of the degenerate gas (e.g., Maeda & Terada 2016; Livio & Mazzali 2018). Given that the majority of Type Ia SNe show standardizable light-curve properties, they are popular standard candles for cosmological distance measurements (e.g., Riess et al. 1998; Perlmutter et al. 1999). In addition to such standardizable “normal” Type Ia SNe, it has been recognized that there are sub-categories in Type Ia SNe, which show a wide range of photometric and spectroscopic properties (e.g., Taubenberger 2017; Jha et al. 2019). These observational diversities are coupled with the different progenitor systems, different evolutionary paths, and/or different thermonuclear burning behavior. However, we have not fully understood the progenitors and explosion mechanisms for different sub-types of Type Ia SNe (e.g., Maoz et al. 2014; Liu et al. 2023).

One of such extremes in Type Ia SNe is so-called 03fg-like (or super-Chandrasekhar) Type Ia SNe, showing different observational properties from “normal” Type Ia SNe (e.g., Howell et al. 2006; Hicken et al. 2007; Scalzo et al. 2010; Yamanaka et al. 2009; Taubenberger et al. 2019; Hsiao et al. 2020; Ashall et al. 2021; Dimitriadis et al. 2023; Srivastav et al. 2023). They

are typically brighter with a peak absolute  $B$ -band magnitude of  $-19 < M_B < -21$  mag (Ashall et al. 2021). In some extreme cases, the required amount of  $^{56}\text{Ni}$  would be similar to the Chandrasekhar-mass ( $\sim 1.4 M_\odot$ ) and thus require super-Chandrasekhar-mass WDs as their progenitors, unless other energy sources significantly contribute to their brightness alike in normal Type Ia SNe (e.g., Yamanaka et al. 2009). They show slow evolution in their light curves (LCs) with  $\Delta m_{15}(B) < 1.3$  mag as well as relatively low expansion velocities ( $8000\text{--}12000 \text{ km s}^{-1}$  for Si II  $\lambda 6355$ ) and strong features from unburnt carbon in their spectra (Ashall et al. 2021), suggesting more massive SN ejecta compared to normal Type Ia SNe (e.g., Taubenberger 2017).

There are several scenarios proposed for explaining the observational properties of the 03fg-like Type Ia SNe. (1) An explosion of a carbon-oxygen (CO) WD whose mass exceeds the Chandrasekhar limit due to its rapid rotation (e.g., Yoon & Langer 2005) and/or strong magnetic fields (e.g., Das & Mukhopadhyay 2013), formed through the accretion from a non-degenerate companion in the single-degenerate scenario (e.g., Whelan & Iben 1973; Nomoto 1982) or through post-merger accretion in the double-degenerate scenario (e.g., Iben & Tutukov 1984; Webbink 1984; Raskin et al. 2014). (2) An explosion of

a CO WD during a merger with a companion WD (the violent merger scenario; e.g., Pakmor 2017, for a review). In this scenario, the high peak luminosity might be achieved due to viewing angle effects of an aspherical explosion (e.g., Hillebrandt et al. 2007; Moll et al. 2014) and/or due to interaction with circumstellar material (CSM; e.g., Hachinger et al. 2012; Noebauer et al. 2016). (3) An explosion after a merger of a WD with the core of a massive asymptotic giant branch star (the core-degenerate scenario; e.g., Sparks & Stecher 1974; Livio & Riess 2003; Kashi & Soker 2011). This scenario may also explain the large brightness with a CSM interaction. It is noted that recent very early-phase (within a few days after the explosion) observations of several 03fg-like SNe have detected early excesses in their LCs, suggesting interaction with H-poor CSM (SNe 2020hvf, 2021zny, 2022ilv and 2022pul; Jiang et al. 2021; Dimitriadis et al. 2023; Srivastav et al. 2023; Siebert et al. 2024). However, the strength of CSM interaction estimated from the observed early excesses is not sufficient to boost the peak brightness from the level of normal Type Ia SNe ( $\sim -19$  mag) to the observed level in bright 03fg-like SNe ( $\sim -20$  mag; e.g., Jiang et al. 2021; Maeda et al. 2023). Therefore, bright 03fg-like SNe still need an additional stronger CSM interaction or super-Chandrasekhar mass  $^{56}\text{Ni}$  as the origin of their extreme brightness.

Nebular-phase observations of the 03fg-like Type Ia SN 2022pul with the James Webb Space Telescope exhibited anti-correlated asymmetric emission-line profiles for the iron-group elements (Fe, Co, Ni) and the intermediate-mass elements (S, Ar, Ca), as well as the presence of strong [Ne II] at  $12.81 \mu\text{m}$  (Kwok et al. 2023; Siebert et al. 2024). The separate distributions of different elements suggest large global ejecta asymmetries in SN 2022pul, and support the violent merger scenario. At the same time, the presence of the strong [Ne II] line was also predicted as a proof of a violent merger scenario by non-local-thermodynamic-equilibrium radiative transfer calculations for various scenarios in Type Ia SNe (Blondin et al. 2023). These discoveries on SN 2022pul strongly support the violent merger scenario for its origin.

Polarimetry provides another powerful way to study the ejecta geometries of SNe. Its application to the 03fg-like Type Ia SNe has been very limited due to the rareness of this class of SNe, but can be the key to understanding their origin. Spectropolarimetric observations of the 03fg-like Type Ia SN 2009dc show low continuum polarization ( $< 0.3\%$ ) and indicate that the explosion is nearly symmetric (Tanaka et al. 2010). This suggests that the explosion mechanism of SN 2009dc is different from that of SN 2022pul, which showed largely aspherical ejecta. Alternatively, this might merely imply that SN 2009dc has a similarly aspherical explosion but with a different viewing angle, i.e., SN 2009dc might be viewed from a direction close to the axis of symmetry. In fact, an aspherical system is expected for SN 2009dc from the line shapes in the nebular spectra (Siebert et al. 2023). Another example is SN 2007if, which shows relatively high wavelength-independent polarization ( $P \sim 0.7\%$ ,  $\theta \sim 130$  degrees) from 13 to 46 days after the brightness peak (Cikota et al. 2019; Chu et al. 2022). Chu et al. (2022) conclude that this polarization likely originates from the interstellar polarization in the Milky Way (MW) as suggested by the relatively high MW extinction, implying that the intrinsic SN polarization is low and thus the explosion should be relatively spherical or viewed from the axis of symmetry. Here, it is noted that the polarization angle of the observed polarization in SN 2007if is not similar with the directions of the interstellar polarization (ISP) of MW stars and the interstellar magnetic fields towards nearby directions from the SN line of sight ( $\sim 40$  degrees, Berdyugin

et al. 2014; Bennett et al. 2013), although the local values do not necessarily follow the global values.

In this paper, we present imaging-polarimetric observations of two 03fg-like Type Ia SNe: SNe 2021zny and 2022ilv (Yamanaka 2021; Burke et al. 2022). SN 2021zny showed several characteristics of the class of 03fg-like Type Ia SNe, such as high peak brightness, slow LC evolution, low ejecta velocities and strong lines from unburnt material (Dimitriadis et al. 2023). Dimitriadis et al. (2023) also report the detection of a flux excess within a few days after the explosion, which can be explained by interaction of the ejecta with  $\sim 0.04 M_{\odot}$  of circumstellar material at a distance of  $\sim 10^{12}$  cm, and prominent [O I]  $\lambda\lambda$  6300, 6364 lines at a late phase. From these observational properties, Dimitriadis et al. (2023) conclude that the origin of SN 2021zny is possibly a merger of two CO WDs, where the disrupted secondary WD ejects carbon-rich CSM before the explosion of the primary WD. Srivastav et al. (2023) demonstrated that SN 2022ilv showed similar photometric and spectroscopic features as 03fg-like Type Ia SNe as well as an early excess in the LC, and also proposed a similar merger scenario as its origin.

## 2. Observations

We conducted *V*- and *R*-band imaging polarimetry using the Alhambra Faint Object Spectrograph and Camera (ALFOSC)<sup>1</sup> on the 2.56m Nordic Optical Telescope (NOT<sup>2</sup>) for 03fg-like Type Ia SNe 2021zny and 2022ilv. The observing logs are shown in Tables 1 and 2. For the linear polarimetry of the SNe, we utilized a half-wave plate (HWP) and a calcite plate. The HWP rotates the polarization axis of the transient light with a certain amount of angle, and then the transient light is split by a calcite plate into two orthogonally polarized beams (the ordinary and extraordinary components). We derived the Stokes parameters from the signals of the ordinary and extraordinary components for 4 HWP angles ( $0^\circ$ ,  $22.5^\circ$ ,  $45^\circ$  and  $67.5^\circ$ ).

The data were reduced and analyzed by the standard methods, e.g., in Patat (2017), using IRAF(Tody 1986, 1993). First, we applied the basic treatment (cosmic-ray removal, bias and flat-field corrections) to all the frames. Then, we performed aperture photometry on the ordinary and the extraordinary components of the transient for all the HWP angles. Since the ordinary and extraordinary beams are overlapped in the ALFOSC images, an artificial polarization signal due to the inhomogeneous structures of the host galaxy and/or the background region can be created. In order to assess such an error for the polarization, we conducted aperture photometry using four different combinations of the aperture size and sky region: (1) an aperture size twice as large as the full width at half maximum (FWHM) of the ordinary beam's point-spread function with a sky region whose inner and outer radii are twice and three times as large as the FWHM; (2) an aperture size twice as large as the FWHM with a sky region whose inner and outer radii are three times and four times as large as the FWHM; (3) an aperture size 2.5 times as large as the FWHM with a sky region whose inner and outer radii are 2.5 times and 3.5 times as large as the FWHM; (4) an aperture size 2.5 times as large as the FWHM with a sky region whose inner and outer radii are 3.5 times and 4.5 times as large as the FWHM. Based on the measurements from the aperture photometry of the ordinary and extraordinary sources for 4 different HWP angles, we derived the Stokes  $q$  and  $u$  values for each combination of the aperture and sky region:  $(q_1 \pm \sigma_{q,1}, u_1 \pm \sigma_{u,1})$ ,  $(q_2 \pm \sigma_{q,2}, u_2 \pm \sigma_{u,2})$ ,

<sup>1</sup> <http://www.not.iac.es/instruments/alfosc/>

<sup>2</sup> <http://www.not.iac.es>

$(q_3 \pm \sigma_{q,3}, u_3 \pm \sigma_{u,3}), (q_4 \pm \sigma_{q,4}, u_4 \pm \sigma_{u,4})$ . Here,  $\sigma$  represents the photon shot noise. Then, we took the average and standard deviation of these  $q$  and  $u$  values as the polarization signal and the error, respectively:

$$q_{\text{ave}} = \frac{\sum_{i=1}^n \left( \frac{q_i}{\sigma_{q,i}^2} \right)}{\sum_{i=1}^n \left( \frac{1}{\sigma_{q,i}^2} \right)}, \sigma_{q,\text{ave}} = \sqrt{\frac{\sum_{i=1}^n \left( \frac{1}{\sigma_{q,i}^2} \right) (q_i - q_{\text{ave}})^2}{(n-1) \sum_{i=1}^n \left( \frac{1}{\sigma_{q,i}^2} \right)}}, \quad (1)$$

$$u_{\text{ave}} = \frac{\sum_{i=1}^n \left( \frac{u_i}{\sigma_{u,i}^2} \right)}{\sum_{i=1}^n \left( \frac{1}{\sigma_{u,i}^2} \right)}, \sigma_{u,\text{ave}} = \sqrt{\frac{\sum_{i=1}^n \left( \frac{1}{\sigma_{u,i}^2} \right) (u_i - u_{\text{ave}})^2}{(n-1) \sum_{i=1}^n \left( \frac{1}{\sigma_{u,i}^2} \right)}}. \quad (2)$$

Here,  $n$  is the number of the measurements to be averaged and  $n = 4$ . From these averaged  $q$  and  $u$  values, we calculated the polarization degree and the polarization angle:

$$P = \sqrt{q_{\text{ave}}^2 + u_{\text{ave}}^2}, \quad (3)$$

$$\begin{aligned} \sigma_P &= \sqrt{\left( \frac{\partial P}{\partial q_{\text{ave}}} \sigma_{q,\text{ave}} \right)^2 + \left( \frac{\partial P}{\partial u_{\text{ave}}} \sigma_{u,\text{ave}} \right)^2} \\ &= \sqrt{\left( \frac{q_{\text{ave}}}{P} \sigma_{q,\text{ave}} \right)^2 + \left( \frac{u_{\text{ave}}}{P} \sigma_{u,\text{ave}} \right)^2}, \end{aligned} \quad (4)$$

$$\chi = \frac{1}{2} \arctan \left( \frac{u_{\text{ave}}}{q_{\text{ave}}} \right), \quad (5)$$

$$\begin{aligned} \sigma_\chi &= \sqrt{\left( \frac{\partial \chi}{\partial q_{\text{ave}}} \sigma_{q,\text{ave}} \right)^2 + \left( \frac{\partial \chi}{\partial u_{\text{ave}}} \sigma_{u,\text{ave}} \right)^2} \\ &= \frac{\sqrt{(u_{\text{ave}} \sigma_{q,\text{ave}})^2 + (q_{\text{ave}} \sigma_{u,\text{ave}})^2}}{2P^2}. \end{aligned} \quad (6)$$

At last, we subtracted the polarization bias from the polarization degrees following the standard method in Wang et al. (1997).

### 3. Results and discussion

Figure 1 shows the time evolution of the  $V$ - and  $R$ -band polarization of SN 2021zny. Both  $V$ - and  $R$ -band polarization shows  $P \sim 0.4\%$  and  $\theta \sim 120$  degrees around the peak. At Phase +29.47 days, the degree of the  $R$ -band polarization is increased to  $\sim 1.9\%$  keeping the polarization angle around  $\sim 120$  degrees, followed by slightly smaller values of the polarization degree and angle at Phase +50.45 days. On the other hand, the  $V$ -band polarization, at Phases +29.47 and +50.45 days, shows small degrees of the polarization ( $\leq 0.5\%$ ) with different polarization angles ( $\sim 45$  degrees) from  $\sim 120$  degrees around the peak. The polarization is also shown in the  $q-u$  plane (Figure 2).

The SN can have not only intrinsic polarization but also ISP. Dimitriadis et al. (2023) estimated the total dust extinction in the Milky Way and in the host galaxy as  $E(B-V)_{\text{tot}} = 0.14 \pm 0.07$  mag for SN 2021zny. The empirical relation by Serkowski et al. (1975) indicates that its ISP should likely have  $P_{\text{max}} \leq 1.3\%$ . From the values of the polarization degree, the polarization component whose angle is  $\sim 45$  degrees (the  $V$ -band polarization at Phases +29.47 and +50.45 days) can be explained to be due to the ISP. This interpretation may naturally explain the discrepancy between the  $V$ - and  $R$ -band polarization at Phases +29.47 and +50.45 days. The  $V$ -band polarization show the ISP due to the line depolarization of the strong continuum polarization,

while the  $R$ -band polarization reflect the strong continuum polarization. Alternatively, the  $V$ -band polarization show the ISP due to the low intrinsic SN continuum polarization, while the  $R$ -band polarization shows a strong line polarization. In this case, the axis of the aspherical distribution of the elements for the strong line polarization should be the same with that of the overall ejecta geometry predicted by the continuum polarization at the first two phases. It is noted that the directions of the magnetic fields, which are supposed to be aligned with the ISP angle (e.g., Davis & Greenstein 1951), in a spiral galaxy tends to follow the directions of the spiral arms (e.g., Beck 2015). Therefore, the polarization angle of this component ( $\theta \sim 45$  degrees), which nicely corresponds to the structure of the host galaxy (see Figure 1 in Dimitriadis et al. 2023), might support this interpretation. Adopting this component ( $P \sim 0.3\%$  and  $\chi \sim 45$  degrees) as the ISP, the  $V$ - and  $R$ -band polarization show both  $\sim 1.0\%$  of the intrinsic polarization around the brightness peak and then  $\sim 0$  and  $\sim 2.0\%$ , respectively, at later phase. Even if this component is another component of the intrinsic SN polarization and the ISP is negligible, the intrinsic polarization is high ( $\sim 1-2\%$ ). The high polarization is on the highest end of the diversity in Type Ia SN polarization or possibly beyond ( $\leq 1\%$ , e.g., Cikota et al. 2019). This indicates that the ejecta of SN 2021zny is significantly aspherical, even compared to the extreme cases of normal Type Ia SNe.

It is noted that there is another possibility for the origin of the continuum polarization in Type Ia SNe, i.e., the polarization due to the scattering by circumstellar dust (e.g., Nagao et al. 2018; Hu et al. 2022). The polarization created by this mechanism has wavelength dependence (typically higher polarization in bluer wavelengths) and time evolution (typically higher polarization at the beginning of the tail phase than at the peak) as demonstrated in Nagao et al. (2018). There are some observational examples (e.g., Yang et al. 2018). Firstly, the polarization in SN 2021zny does not show clear wavelength dependence at Phases +29.47 and +50.45 days, while it shows higher degrees in the  $R$  band than those in the  $V$  band at latter phase. Secondly, SN 2021zny shows relatively high polarization degrees already before the  $B$ -band peak ( $\sim 0.4\%$  at Phase -6.33). These features cannot be explained with the dust scattering scenario. Therefore, we reject the possibility of scattering in circumstellar dust as the origin of the polarization in SN 2021zny.

Figure 3 shows the time evolution of the  $V$ - and  $R$ -band polarization in SN 2022ilv. The polarization degrees are high and time-variable around  $\sim 2.0\%$  with a relatively constant polarization angle of around  $\sim 60$  degrees, except for the data at Phase +60.48 days ( $P \sim 0.5\%$ ,  $\theta \sim 30$  degrees). The polarization degrees and angles in the  $V$  and  $R$  bands are relatively consistent at all phases except Phase +5.54, indicating wavelength-independent polarization, i.e., continuum polarization rather than line polarization. The polarization at Phase +5.54 may be due to the effects of line polarization and depolarization. This behavior of the polarization is also seen in the  $q-u$  plane (Figure 4), although the early-phase points are clustered around a point deviating from the points at Phase +60.48 days, except the  $R$ -band point at Phase +5.54.

Srivastav et al. (2023) estimated the dust extinction for SN 2022ilv to be  $E(B-V)_{\text{tot}} = 0.11$  mag, assuming that the extinction arises only from the MW dust because the host galaxy is extremely faint and thus should have a low metallicity and small amount of dust. Adopting this value, the empirical relation by Serkowski et al. (1975) indicates that its ISP should have  $P_{\text{max}} \leq 1.0\%$ . Given that the observed polarization around the peak is too high to be dominated by the ISP, it should be domi-

**Table 1.** Log of the imaging-polarimetric observations of SN 2021zny and their measurements.

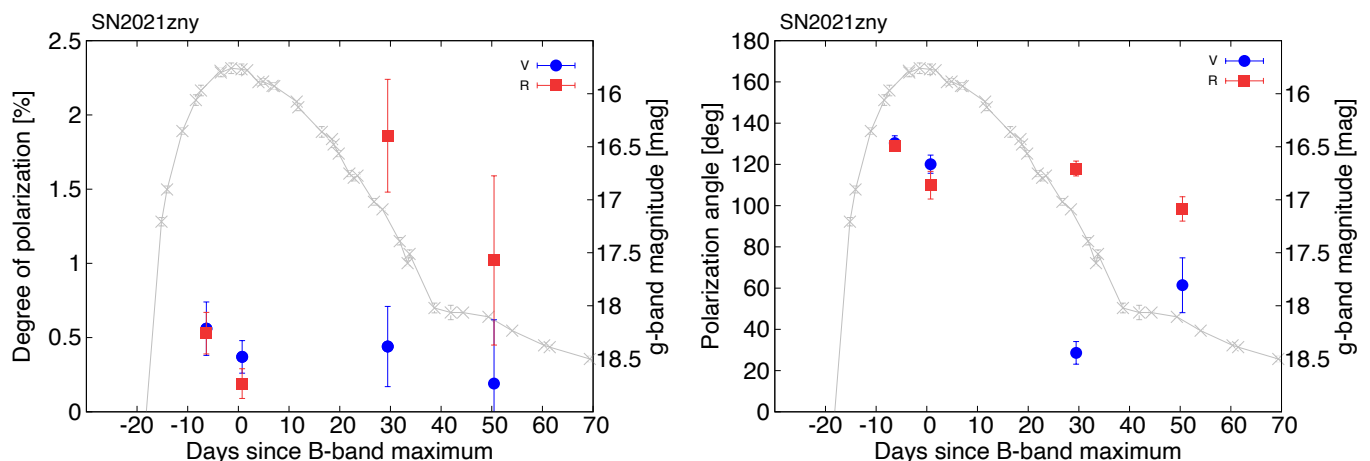
Date (UT)	MJD (days)	Phase <sup>a</sup> (days)	Exp. time (seconds)	$q_{ave}$ (%)	$u_{ave}$ (%)	Pol. degree (%)	Pol. angle (degree)	Filter
2021-10-05.13	59492.13	-6.33	4 × 80	-0.10 ± 0.15	-0.60 ± 0.18	0.56 ± 0.18	130.3 ± 3.6	V
			4 × 80	-0.12 ± 0.05	-0.55 ± 0.14	0.53 ± 0.14	128.8 ± 1.5	R
2021-10-12.20	59499.20	+0.74	4 × 50	-0.20 ± 0.13	-0.35 ± 0.10	0.37 ± 0.11	120.1 ± 4.4	V
			4 × 50	-0.18 ± 0.07	-0.15 ± 0.13	0.19 ± 0.10	109.9 ± 6.7	R
2021-11-09.93	59527.93	+29.47	4 × 120	0.31 ± 0.14	0.48 ± 0.31	0.44 ± 0.27	28.6 ± 5.1	V
			4 × 80	-1.08 ± 0.57	-1.60 ± 0.24	1.86 ± 0.38	118.0 ± 3.6	R
2021-11-30.91	59548.91	+50.45	4 × 120	-0.29 ± 0.54	0.45 ± 0.37	0.19 ± 0.43	61.4 ± 13.3	V
			4 × 100	-1.22 ± 0.57	-0.37 ± 0.52	1.02 ± 0.57	98.4 ± 5.9	R

Notes. <sup>a</sup>Relative to the *B*-band peak:  $t_0 = 59498.46$  (MJD Dimitriadis et al. 2023).

**Table 2.** Log of the imaging-polarimetric observations of SN 2022ilv and their measurements.

Date (UT)	MJD (days)	Phase <sup>a</sup> (days)	Exp. time (seconds)	$q_{ave}$ (%)	$u_{ave}$ (%)	Pol. degree (%)	Pol. angle (degree)	Filter
2022-05-03.18	59702.18	-5.28	4 × 80	-1.00 ± 0.03	1.50 ± 0.07	1.80 ± 0.06	61.8 ± 0.4	V
			4 × 80	-0.97 ± 0.11	1.88 ± 0.15	2.11 ± 0.14	58.6 ± 0.8	R
2022-05-14.00	59713.00	+5.54	4 × 80	-1.57 ± 0.19	1.95 ± 0.07	2.50 ± 0.13	64.4 ± 0.9	V
			4 × 80	0.14 ± 0.57	1.16 ± 0.40	1.03 ± 0.40	41.6 ± 7.0	R
2022-06-03.95	59733.95	+26.49	4 × 100	-1.27 ± 0.17	1.26 ± 0.30	1.76 ± 0.24	67.6 ± 2.0	V
			4 × 100	-1.14 ± 0.08	0.64 ± 0.11	1.30 ± 0.09	75.3 ± 1.1	R
2022-06-26.96	59756.96	+49.50	4 × 120	-1.57 ± 0.09	0.29 ± 0.20	1.59 ± 0.10	84.8 ± 1.8	V
			4 × 100	-1.23 ± 0.19	1.83 ± 0.58	2.09 ± 0.49	62.0 ± 2.3	R
2022-07-07.94	59767.94	+60.48	4 × 120	0.55 ± 0.45	0.49 ± 0.16	0.57 ± 0.35	20.8 ± 6.3	V
			4 × 120	0.35 ± 0.66	1.49 ± 0.99	0.91 ± 0.98	38.4 ± 6.4	R

Notes. <sup>a</sup>Relative to the *g*-band peak:  $t_0 = 59707.46$  (MJD Srivastav et al. 2023).


**Fig. 1.** Polarization degree and angle of the *V*- (blue circle) and *R*-band (red square) polarization in SN 2021zny. The gray crosses connected with lines show the *g*-band LC of SN 2021zny from Dimitriadis et al. (2023).

nated by the intrinsic SN polarization. The polarization degrees at Phase +60.48 days can be consistent with the ISP. However, the polarization angle of the ISP in the MW along the line of sight to SN 2022ilv is estimated to be  $\sim 130$  degrees by polarimetric observations of MW stars at  $\sim 100$ – $\sim 600$  pc (Figure 3 in Berdyugin et al. 2014). Given that the MW extinction

for SN 2022ilv is mainly caused by dust at  $\leq 140$  pc (Green et al. 2019), the ISP can be estimated to be  $\leq 1.0$  and  $\sim 0.5\%$  as an averaged value (Figure 4 in Berdyugin et al. 2014). Therefore, we conclude that the ISP is negligible ( $\leq 0.5\%$ ) and the polarization at Phase +60.48 days might still express another intrinsic component with a slightly different angle ( $P \sim 0.5\%$ ,

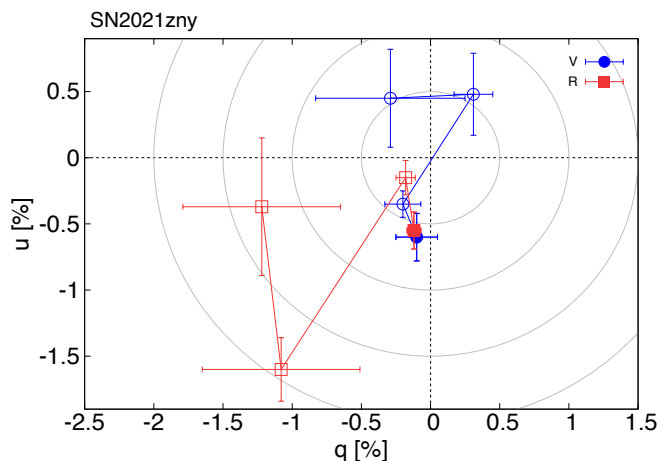


**Fig. 2.** The time evolution of the V- (blue) and R-band (red) polarization in SN 2021zny in the  $q-u$  plane. The first-epoch (Phase -6.33 days) data are shown with filled points. The gray lines correspond to the polarization degrees of 0.5, 1.0 and 1.5 % from the origin, respectively.

$\theta \sim 30$  degrees), in addition to the intrinsic component at the early phases ( $\sim 2.0$  % and  $\sim 60$  degrees). This might indicate inhomogeneous structures in the SN ejecta. Even if we assume that the polarization at Phase +60.48 days is dominated by the ISP, the ISP-subtracted intrinsic SN polarization at early phases is high ( $P \sim 2.0$  %). It is noted that, as in the case of SN 2021zny, the polarization in SN 2021ilv also cannot be explained by the scattering in circumstellar dust. In any case, the intrinsic SN polarization is very high  $\sim 2$  %, which is the highest intrinsic continuum polarization observed in any Type Ia SN (e.g., Wang & Wheeler 2008; Cikota et al. 2019). This implies that the ejecta of SN 2022ilv is also very aspherical, compared to any other Type Ia SNe.

The V- and R-band polarization in SNe 2021zny and 2022ilv shows high degrees ( $\sim 1 - \sim 2\%$ ), indicating large aspherical structures. According to the numerical calculations of the polarization signal in various scenarios for Type Ia SNe by Bulla et al. (2016b,a), the only possible scenario to show such high polarization, i.e., a large aspherical structure, is the violent merger scenario. Even though the aspherical structures in the 03fg-like Type Ia SNe have been suggested using several different modes of observations (see Section 1), our observations provide the first evidence from polarimetry for such aspherical structures.

**Acknowledgements.** We thank Masayuki Yamanaka for helpful discussions. This work is based on observations made under program IDs P64-023, P65-004 and P65-005 with the Nordic Optical Telescope, owned in collaboration by the University of Turku and Aarhus University, and operated jointly by Aarhus University, the University of Turku and the University of Oslo, representing Denmark, Finland and Norway, the University of Iceland and Stockholm University at the Observatorio del Roque de los Muchachos, La Palma, Spain, of the Instituto de Astrofísica de Canarias. TN acknowledges support from the Research Council of Finland projects 324504, 328898 and 353019. KM acknowledges support from the Japan Society for the Promotion of Science (JSPS) KAKENHI grant (JP20H00174 and JP24H01810) and by the JSPS Open Partnership Bilateral Joint Research Project between Japan and Finland (JPJSBP120229923). S. M. was funded by the Research Council of Finland project 350458. HK was funded by the Research Council of Finland projects 324504, 328898, and 353019. CPG acknowledges financial support from the Secretary of Universities and Research (Government of Catalonia) and by the Horizon 2020 Research and Innovation Programme of the European Union under the Marie Skłodowska-Curie and the Beatriu de Pinós 2021 BP 00168 programme, from the Spanish Ministerio de Ciencia e Innovación (MCIN) and the Agencia Estatal de Investigación (AEI) 10.13039/501100011033 under the PID2020-115253GA-I00 HOSTFLOWS project, and the program Unidad de Excelencia María de Maeztu CEX2020-001058-M.

## References

- Ashall, C., Lu, J., Hsiao, E. Y., et al. 2021, *ApJ*, 922, 205  
 Beck, R. 2015, *A&A Rev.*, 24, 4  
 Bennett, C. L., Larson, D., Weiland, J. L., et al. 2013, *ApJS*, 208, 20  
 Berdyugin, A., Piirola, V., & Teerikorpi, P. 2014, *A&A*, 561, A24  
 Blondin, S., Dessart, L., Hillier, D. J., Ramsbottom, C. A., & Storey, P. J. 2023, *A&A*, 678, A170  
 Bulla, M., Sim, S. A., Kromer, M., et al. 2016a, *MNRAS*, 462, 1039  
 Bulla, M., Sim, S. A., Pakmor, R., et al. 2016b, *MNRAS*, 455, 1060  
 Burke, J., Howell, D. A., McCully, C., et al. 2022, *Transient Name Server Classification Report*, 2022-1137, 1  
 Chu, M. R., Cikota, A., Baade, D., et al. 2022, *MNRAS*, 509, 6028  
 Cikota, A., Patat, F., Wang, L., et al. 2019, *MNRAS*, 490, 578  
 Das, U. & Mukhopadhyay, B. 2013, *Phys. Rev. Lett.*, 110, 071102  
 Davis, Leverett, J. & Greenstein, J. L. 1951, *ApJ*, 114, 206  
 Dimitriadis, G., Maguire, K., Karambelkar, V. R., et al. 2023, *MNRAS*, 521, 1162  
 Green, G. M., Schlafly, E., Zucker, C., Speagle, J. S., & Finkbeiner, D. 2019, *ApJ*, 887, 93  
 Hachinger, S., Mazzali, P. A., Taubenberger, S., et al. 2012, *MNRAS*, 427, 2057  
 Hicken, M., Garnavich, P. M., Prieto, J. L., et al. 2007, *ApJ*, 669, L17  
 Hillebrandt, W., Sim, S. A., & Röpke, F. K. 2007, *A&A*, 465, L17  
 Howell, D. A., Sullivan, M., Nugent, P. E., et al. 2006, *Nature*, 443, 308  
 Hsiao, E. Y., Hoefflich, P., Ashall, C., et al. 2020, *ApJ*, 900, 140  
 Hu, M., Wang, L., & Wang, X. 2022, *ApJ*, 931, 110  
 Iben, I. J. & Tutukov, A. V. 1984, *ApJS*, 54, 335  
 Jha, S. W., Maguire, K., & Sullivan, M. 2019, *Nature Astronomy*, 3, 706  
 Jiang, J.-a., Maeda, K., Kawabata, M., et al. 2021, *ApJ*, 923, L8  
 Kashi, A. & Soker, N. 2011, *MNRAS*, 417, 1466  
 Kwok, L. A., Siebert, M. R., Johansson, J., et al. 2023, *arXiv e-prints*, arXiv:2308.12450  
 Liu, Z.-W., Röpke, F. K., & Han, Z. 2023, *Research in Astronomy and Astrophysics*, 23, 082001  
 Livio, M. & Mazzali, P. 2018, *Phys. Rep.*, 736, 1  
 Livio, M. & Riess, A. G. 2003, *ApJ*, 594, L93  
 Maeda, K., Jiang, J.-a., Doi, M., Kawabata, M., & Shigeyama, T. 2023, *MNRAS*, 521, 1897  
 Maeda, K. & Terada, Y. 2016, *International Journal of Modern Physics D*, 25, 1630024  
 Maoz, D., Mannucci, F., & Nelemans, G. 2014, *ARA&A*, 52, 107  
 Moll, R., Raskin, C., Kasen, D., & Woosley, S. E. 2014, *ApJ*, 785, 105  
 Nagao, T., Maeda, K., & Yamanaka, M. 2018, *MNRAS*, 476, 4806  
 Noebauer, U. M., Taubenberger, S., Blinnikov, S., Sorokina, E., & Hillebrandt, W. 2016, *MNRAS*, 463, 2972  
 Nomoto, K. 1982, *ApJ*, 253, 798  
 Pakmor, R. 2017, in *Handbook of Supernovae*, ed. A. W. Alsabti & P. Murdin, 1257  
 Patat, F. 2017, in *Handbook of Supernovae*, ed. A. W. Alsabti & P. Murdin, 1017  
 Perlmutter, S., Aldering, G., Goldhaber, G., et al. 1999, *ApJ*, 517, 565  
 Raskin, C., Kasen, D., Moll, R., Schwab, J., & Woosley, S. 2014, *ApJ*, 788, 75  
 Riess, A. G., Filippenko, A. V., Challis, P., et al. 1998, *AJ*, 116, 1009  
 Scalzo, R. A., Aldering, G., Antilogus, P., et al. 2010, *ApJ*, 713, 1073  
 Serkowski, K., Mathewson, D. S., & Ford, V. L. 1975, *ApJ*, 196, 261  
 Siebert, M. R., Foley, R. J., Zenati, Y., et al. 2023, *ApJ*, 958, 173  
 Siebert, M. R., Kwok, L. A., Johansson, J., et al. 2024, *ApJ*, 960, 88  
 Sparks, W. M. & Stecher, T. P. 1974, *ApJ*, 188, 149  
 Srivastav, S., Smartt, S. J., Huber, M. E., et al. 2023, *ApJ*, 943, L20  
 Tanaka, M., Kawabata, K. S., Yamanaka, M., et al. 2010, *ApJ*, 714, 1209  
 Taubenberger, S. 2017, in *Handbook of Supernovae*, ed. A. W. Alsabti & P. Murdin, 317  
 Taubenberger, S., Floers, A., Vogl, C., et al. 2019, *MNRAS*, 488, 5473  
 Tody, D. 1986, in *Society of Photo-Optical Instrumentation Engineers (SPIE) Conference Series*, Vol. 627, *Instrumentation in astronomy VI*, ed. D. L. Crawford, 733  
 Tody, D. 1993, in *Astronomical Society of the Pacific Conference Series*, Vol. 52, *Astronomical Data Analysis Software and Systems II*, ed. R. J. Hanisch, R. J. V. Brissenden, & J. Barnes, 173  
 Wang, L. & Wheeler, J. C. 2008, *ARA&A*, 46, 433  
 Wang, L., Wheeler, J. C., & Höflich, P. 1997, *ApJ*, 476, L27  
 Webbink, R. F. 1984, *ApJ*, 277, 355  
 Whelan, J. & Iben, I. 1973, *ApJ*, 186, 1007  
 Yamanaka, M. 2021, *Transient Name Server Classification Report*, 2021-3361, 1  
 Yamanaka, M., Kawabata, K. S., Kinugasa, K., et al. 2009, *ApJ*, 707, L118  
 Yang, Y., Wang, L., Baade, D., et al. 2018, *ApJ*, 854, 55  
 Yoon, S. C. & Langer, N. 2005, *A&A*, 435, 967

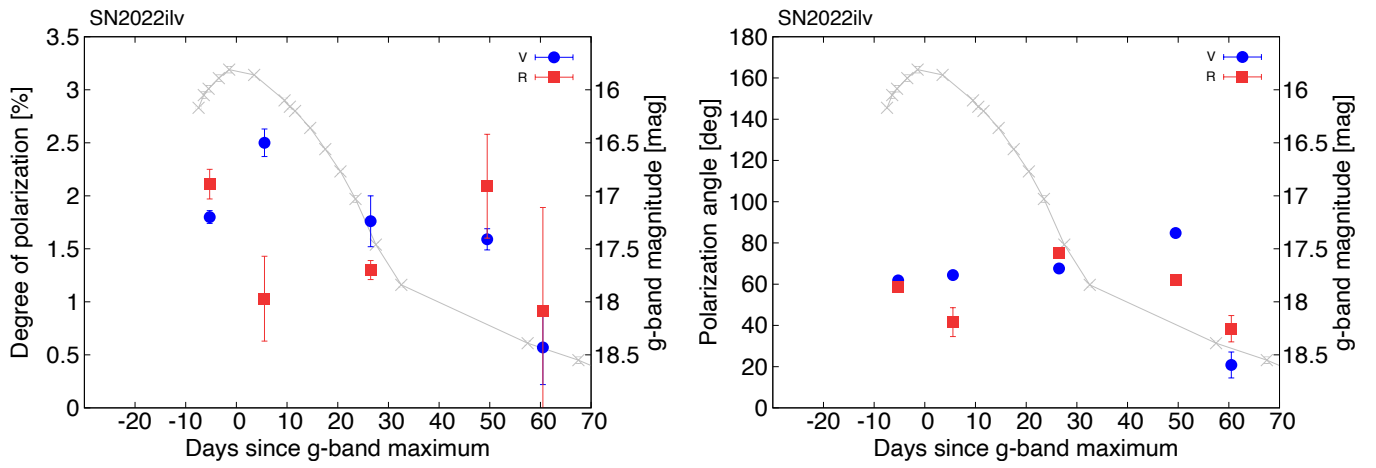


**Fig. 3.** Same as Figure1 but for SN 2022ilv. The gray dots connected with lines show the  $g$ -band LC of SN 2022ilv from Srivastav et al. (2023).

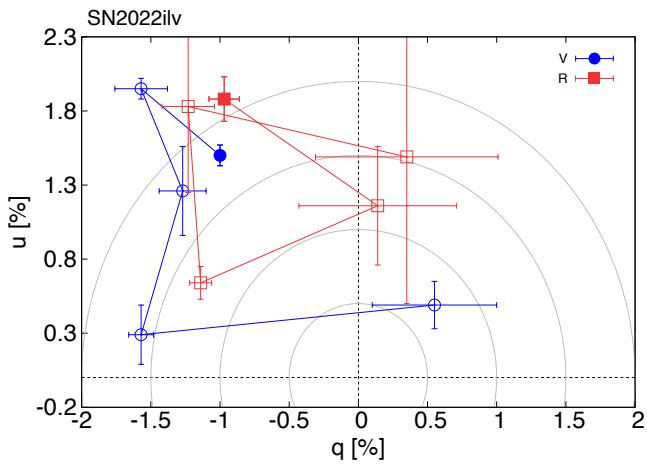


**Fig. 4.** Same as Figure2 but for SN 2022ilv. The gray lines correspond to the polarization degrees of 0.5, 1.0, 1.5 and 2.0 % from the origin, respectively.